



Article

Beamspace Scene Classification Algorithm for Low-Angle Estimation in MIMO Radar

Sheng Chen , Yongbo Zhao *, Yili Hu and Ben Niu

National Laboratory of Radar Signal Processing, Xidian University, Xi'an 710071, China; shengchen@stu.xidian.edu.cn (S.C.); huyili66@stu.xidian.edu.cn (Y.H.); bniuxd@stu.xidian.edu.cn (B.N.)
* Correspondence: ybzhao@xidian.edu.cn

Abstract: This paper discusses the issue of low-angle estimation in multiple-input, multiple-output (MIMO) radar. Due to the low amount of data transmission, storage, and computation required for beamspace super-resolution algorithms in low-angle estimation, the method has gained considerable interest in recent years. This paper develops a beamspace scene classification (BSC) algorithm to enhance the performance of low-angle estimation in MIMO radar. The proposed BSC algorithm solves an initial angle estimate and the multipath coefficient estimate using the 3D beamspace data, and further constructs the beamspace data required for transmitting and receiving sides to reduce the data dimensions. It is additionally used to provide three estimation schemes with closed-form solutions for three multipath scenes (obtaining two estimations for transmitting and receiving sides). Finally, it fuses the estimates of the two sides by the minimum variance criterion. As a result, the proposed method achieves high estimation accuracy while requiring few processing resources. Moreover, the computational complexity of the proposed algorithm is examined in this study, with the results demonstrating that the proposed method is superior for engineering applications.

Keywords: low-angle tracking; MIMO radar; data fusion; beamspace processing; undulating reflecting surface; multipath signal



Citation: Chen, S.; Zhao, Y.; Hu, Y.; Niu, B. Beamspace Scene Classification Algorithm for Low-Angle Estimation in MIMO Radar. *Remote Sens.* **2022**, *14*, 1917. <https://doi.org/10.3390/rs14081917>

Academic Editors: Junjie Wu, Xiaolong Chen, Jibin Zheng and Bo Chen

Received: 13 March 2022

Accepted: 14 April 2022

Published: 15 April 2022

Publisher's Note: MDPI stays neutral with regard to jurisdictional claims in published maps and institutional affiliations.



Copyright: © 2022 by the authors. Licensee MDPI, Basel, Switzerland. This article is an open access article distributed under the terms and conditions of the Creative Commons Attribution (CC BY) license (<https://creativecommons.org/licenses/by/4.0/>).

1. Introduction

Low-angle estimation in multipath environments has received considerable attention in recent decades [1–5] due to the multipath effect. Direct and reflected signals traveling through the earth's surface are combined in the radar's primary beam. Because the direct and reflected signals return from the same distance unit and enter the main beam of the radar antenna simultaneously, they are difficult to differentiate, resulting in a loss of low-angle estimation performance. Multiple-input, multiple-output (MIMO) radars [6–11] have a higher spatial resolution [12] than phased array radars with the same target resources. MIMO radars can be classified according to their antenna distribution into collocated [6] and widely distributed [7,8] categories. In any case, MIMO radar suffers from the obvious disadvantage of requiring significant quantities of data to be transferred, stored, and computed. Effective dimensionality-reduction techniques, such as beamspace processing [13–17], have garnered much interest, and are excellent contenders for MIMO radar. Additionally, the signal model cannot be developed accurately for the undulating reflecting surface, resulting in a degradation of the conventional low-angle estimation performance [18]. Thus, this paper discusses the beamspace low-angle estimation approach for MIMO radar with a collocated antenna beneath the undulating reflecting surface.

Currently, approaches with high resolution, such as subspace algorithms and maximum likelihood (ML) algorithm, are effective at solving the problem of low-angle estimation. Subspace algorithms, such as MUSIC [19,20] and ESPRIT [21,22], typically require additional snapshots, and fail to directly address coherent signals. Despite the potential for spatial smoothing in solving conventional coherent signals, their performance in

MIMO radar is suboptimal [23,24], because multipath signals in MIMO radar are more sophisticated than conventional coherent signals. ML algorithms [25] are capable of processing coherent signals directly and operating with only one snapshot. Additionally, the root-mean-squared error (RMSE) of the ML algorithm is approximately identical to the Cramer–Rao bound (CRB) [5]. Thus, it is more desirable for low-angle estimates. However, ML algorithms often demand multi-dimensional search with a high computational cost. The beamspace-improved ML (BIML) algorithm [24] for MIMO radar is proposed for low-angle estimation. The BIML algorithm is insensitive to environmental errors and transforms the data from element-space to beamspace. The simulation results indicate that with three transmitting beams and three receiving beams, the method can achieve high performance. However, the computational burden still needs to be further reduced for MIMO radar. The search-free beamspace ML (SF-BML) algorithm for phase array radar [2,3] solves the low-angle estimation problem using 3D beamspace data. In the SF-BML algorithm, the one-dimensional noise subspace is orthogonal to the two-dimensional signal subspace. With this feature, SF-BML provides a closed-form solution for angle estimation. SF-BML is particularly beneficial for engineering applications due to its low computational complexity. By converting MIMO radar data to phase radar data, the 3D beamspace ML fusion (3D-BMLF) algorithm in [26] obtains the indirect closed-form solution for bistatic MIMO radar. The 3D-BMLF algorithm estimates angles at a low computational cost, demonstrating that the closed-form solution is comparable to the numerical solution in terms of accuracy. The refined maximum likelihood (RML) algorithm [27,28] employs the refined signal model in conjunction with prior knowledge of geometric information and the surface reflection coefficient. Additionally, it utilizes composite guide vectors instead of conventional guide vectors to provide an accurate estimation. In this way, the RML algorithm can alleviate the computational burden to a certain extent and enhance the estimation accuracy. The reduced-dimension RML algorithm for MIMO radar [29] transmits beamspace signals and receives element-space signals to reduce the computational costs. The beamspace phase solving (BPS) algorithm [30] solves the angle via the multipath coefficient without searching, where the multipath coefficient concludes the reflection coefficient and the phase difference between direct and multipath signals. The BPS algorithm utilizes the same information as the RML algorithm, but requires less processing to achieve the same degree of accuracy.

Although the RML and BPS algorithms have high estimation accuracy, and the BPS algorithm can estimate multipath coefficient in beamspace, their angle-estimation performance is sensitive to environmental errors caused by the refined signal model mismatch [18]. Due to the scarcity of beamspace low-angle estimation methods for complex scenes, element-space methods are introduced here. Although the reflection coefficient can be estimated offline [31], the actual reflection coefficient is dependent on factors such as elevation angle, operation frequency, and surface vegetation, making the offline estimation coefficient inaccurate. The multipath coefficient can also be estimated using eigendecomposition [32,33], but multiple snapshots are required in this case. Xie et al. [34] considered the condition in which some incident direct signals from various directions are coherent. The multi-dimensional search has also been considered for complex terrain [18,35–37]. Wang et al. [18] assessed the angle and reflection-surface height together to improve robustness. Liu [35] estimated both the angle and multipath coefficient simultaneously. Liu et al. [36] estimated the direct and multipath angles as well as the multipath coefficient jointly. Additionally, Song et al. [37] evaluated the precise signal model based on each array element when estimating the low angle under the undulating reflecting surface. However, their proposed approach requires a large number of searches. Additionally, low-angle estimations developed based on compressive sensing demonstrated high accuracy of estimation [38,39]. These models make use of alternative optimization and dictionary updating techniques to appropriately reduce the computational burden. However, due to the complexity of parameter selection and the limitations on reducing computational burden, these methods are cumbersome to use at present. These methods typically rely

on searching for additional parameters to enhance their robustness. Thus, the majority of these methods are computationally expensive, particularly for MIMO radar.

In summary, there are few methods suited for undulating reflecting surfaces and MIMO radar [24,26], and none of them can combine high precision with low processing cost. In this paper, a beamspace scene classification (BSC) algorithm is developed for low-angle estimation in MIMO Radar. To begin, the BSC algorithm utilizes the 3D beamspace data to solve an initial estimate according to the idea of 3D-BMLF. Following that, the BSC algorithm solves the multipath coefficient using the 3D beamspace data and determines the strength of the multipath component based on the multipath coefficient. Afterwards, appropriate beamspace data are constructed for the transmitting and receiving sides. Then, if the multipath component is sufficiently strong, BSC uses 3D beamspace data to solve two target angle solutions based on the refined signal model; if the multipath component is relatively weak, BSC uses 3D beamspace data to solve two target angle solutions based on SF-BML; while if the multipath component is very weak, BSC uses 2D beamspace data to solve two solutions according to the idea of [3]. Finally, BSC fuses the two solutions by minimizing the mean square error (MSE) while taking into account the estimated multipath coefficient. The simulation results demonstrate that the proposed method achieves high estimation accuracy while being computationally efficient and insensitive to parameter errors.

The proposed method introduces novelties in five distinct ways. First, using 3D beamspace data to solve the multipath coefficient for MIMO radar; second, effectively constructing beamspace data for transmitting and receiving sides; third, developing a scene-classification strategy based on the multipath coefficient, which takes into account the case of flat terrain and undulating terrain; fourth, using 3D beamspace data to solve the closed-form solution of the target angle based on a refined signal model for MIMO radar; and fifth, using 2D beamspace data to solve the closed-form solution of the target angle with no multipath signal for MIMO radar.

The remainder of this paper is organized as follows: Section 2 discusses the details of a multipath signal model and proposes the BSC algorithm. Section 3 presents a computer simulation of the proposed algorithm. Section 4 discusses the simulation results and examines the computational complexity of the proposed algorithms. Finally, Section 5 concludes the paper.

Table 1 defines the symbols in this paper.

Table 1. Related notations.

Notations	Definitions
$[\cdot]^T$	transpose
$[\cdot]^*$	conjugate
$[\cdot]^H$	Conjugate–transpose
$\ \cdot\ _2$	L_2 norm
$\text{Re}\{\cdot\}$	the real part operator
$\text{Im}\{\cdot\}$	the imagery part operator
$\arcsin[\cdot]$	the arcsine operator
$\arctan[\cdot]$	the arctangent operator
$(\cdot)^+$	the Moore–Penrose inverse operator
$\langle \cdot \rangle$	the rounding operator
$[\cdot]^\perp$	the orthocomplement of a projector matrix

2. Method

This section introduces the multipath signal model and presents the proposed BSC algorithm appropriate for beamspace low-angle estimation in MIMO radar under the undulating reflecting surface. The BSC algorithm estimates the initial angle and multipath coefficient, and further provides a scenario classification policy. Then, the BSC algorithm constructs the beamspace data required for transmitting and receiving sides, and finally provides specific solutions.

2.1. Multipath Signal Model

Consider a narrowband collocated MIMO radar equipped with a uniform linear array. The geometry for the low-angle estimation scenario is illustrated in Figure 1. The linear array with M_t transmit elements and M_r receive elements is mounted vertically in the horizontal plane. The array radar center is elevated to h_r . The distance between two adjacent array elements is d . The signals transmitted by the antenna reach the target through two paths: the direct path and the reflection path through the reflector. The signals reflected by the target also reach the antenna through the same two paths. Both pathways are oriented in the direction of θ_1 and θ_2 , respectively. The height of the target is h_t . The distance from the target to the array radar center is R_d .

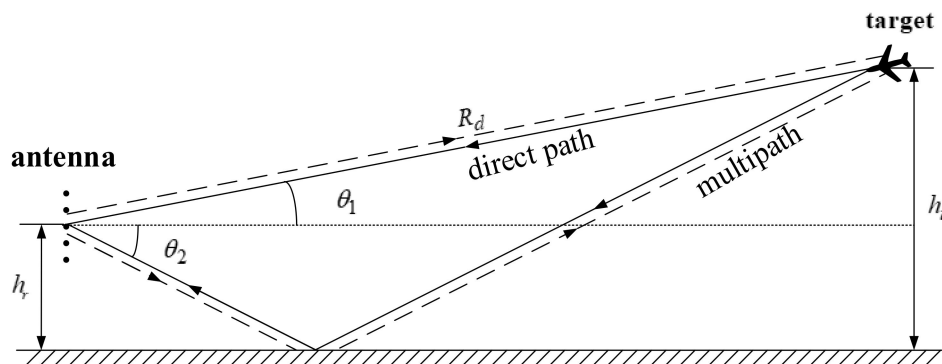


Figure 1. Geometry for the low-angle estimation scenario in MIMO radar.

For the MIMO radar system, the received signal in element space is denoted by [24]

$$X = \alpha b_r(\theta_1) b_t^T(\theta_1) S + N \tag{1}$$

where $X \in C^{M_r \times L}$, L is the number of snapshots, α is the complex amplitude involving the target scattering coefficient, path losses, and so on, and $S \in C^{M_t \times L}$ is the transmitted waveform. $b_r(\theta_1) \in C^{M_r \times 1}$ and $b_t(\theta_1) \in C^{M_t \times 1}$ are the composite-receiver and the composite-transmitter array steering vectors, respectively, including direct and multipath signals, expressed as

$$b_r(\theta_1) = [a_r(\theta_1) \quad a_r(\theta_2)] \begin{bmatrix} 1 \\ \varepsilon \end{bmatrix} \tag{2}$$

$$b_t(\theta_1) = [a_t(\theta_1) \quad a_t(\theta_2)] \begin{bmatrix} 1 \\ \varepsilon \end{bmatrix} \tag{3}$$

where

$$a_r(\theta) = \left[\exp\left(-\frac{j\pi d(M_r - 1) \sin \theta}{\lambda}\right), \exp\left(-\frac{j\pi d(M_r - 3) \sin \theta}{\lambda}\right), \dots, \exp\left(\frac{j\pi d(M_r - 1) \sin \theta}{\lambda}\right) \right]^T \tag{4}$$

$$a_t(\theta) = \left[\exp\left(-\frac{j\pi d(M_t - 1) \sin \theta}{\lambda}\right), \exp\left(-\frac{j\pi d(M_t - 3) \sin \theta}{\lambda}\right), \dots, \exp\left(\frac{j\pi d(M_t - 1) \sin \theta}{\lambda}\right) \right]^T \tag{5}$$

$$\varepsilon = \rho e^{-j\varphi(\theta_1)} = |\rho| e^{j\psi(\theta_1)} \tag{6}$$

$$\psi(\theta_1) = \phi_\rho - \varphi(\theta_1) = \phi_\rho - \frac{4\pi h_r (\sin \theta_1 + h_r / R_d)}{\lambda} \tag{7}$$

where λ is the working wavelength, ε is the multipath coefficient, ρ is the surface reflection coefficient, which is the product of the smooth surface reflection coefficient, the divergence factor, and the surface roughness factor [27], and ϕ_ρ is the phase of ρ . $N \in C^{M_r \times L}$ is the Gaussian white noise vector with a zero mean, which is independent of the target signals.

The noise power of a single element is σ_n^2 . Additionally, given the geometric relationship illustrated in Figure 1, θ_2 can be simply determined by

$$\theta_2 = f(\theta_1) = -\arcsin(\sin(\theta_1) + 2h_r/R_d) \quad (8)$$

Actually, multipath reflection signals are not limited to only one path, but are equivalent to the echo in the Fresnel reflection area [40,41], with a broad spatial extent. Therefore, even if the reflection surface is complex, the equivalent reflection echo direction will not deviate much from the direction $f(\theta_1)$.

For the orthogonal signals, $\mathbf{R}_s = \mathbf{S}\mathbf{S}^H/L$ is an invertible matrix. Using $\tilde{\mathbf{S}} = \mathbf{R}_s^{-1}\mathbf{S}/\sqrt{L}$ to process the echo signal by matched-filtering, the output of the matched-filter can be derived as

$$\mathbf{Y} = \mathbf{X}\tilde{\mathbf{S}}^H = \alpha\mathbf{b}_r(\theta_1)\mathbf{b}_t^T(\theta_1)\mathbf{S}\tilde{\mathbf{S}}^H + \mathbf{N}\tilde{\mathbf{S}}^H = \alpha\sqrt{L}\mathbf{b}_r(\theta_1)\mathbf{b}_t^T(\theta_1) + \mathbf{N}_{s0} \quad (9)$$

where $\mathbf{Y} \in \mathbb{C}^{M_r \times M_t}$ and $\mathbf{N}_{s0} \in \mathbb{C}^{M_r \times M_t}$. Considering an $M_t \times 3$ orthogonal transmit beamformer \mathbf{T}_t and an $M_r \times 3$ orthogonal receive beamformer \mathbf{T}_r as

$$\mathbf{T}_t = \begin{bmatrix} \mathbf{a}_t(-\theta_t) & \mathbf{a}_t(0) & \mathbf{a}_t(\theta_t) \end{bmatrix} \quad (10)$$

$$\mathbf{T}_r = \begin{bmatrix} \mathbf{a}_r(-\theta_r) & \mathbf{a}_r(0) & \mathbf{a}_r(\theta_r) \end{bmatrix} \quad (11)$$

where $\theta_t = \arcsin(\lambda/dM_t)$ and $\theta_r = \arcsin(\lambda/dM_r)$, the target data in 3D beamspace is formed as

$$\mathbf{Y}_B = \alpha\sqrt{L}\mathbf{b}_{Br}(\theta_1)\mathbf{b}_{Bt}^T(\theta_1) + \mathbf{N}_s = \begin{bmatrix} \mathbf{Y}_{:,1}^B & \mathbf{Y}_{:,2}^B & \mathbf{Y}_{:,3}^B \end{bmatrix} = \begin{bmatrix} \mathbf{Y}_{1,:}^B \\ \mathbf{Y}_{2,:}^B \\ \mathbf{Y}_{3,:}^B \end{bmatrix} \quad (12)$$

where $\mathbf{b}_{Br}(\theta_1) = \mathbf{T}_r^H\mathbf{b}_r(\theta_1)$, $\mathbf{b}_{Bt}(\theta_1) = \mathbf{T}_t^H\mathbf{b}_t(\theta_1)$, and $\mathbf{N}_s = \mathbf{T}_r^H\mathbf{N}_{s0}\mathbf{T}_t^*$. The three columns of \mathbf{Y}_B : $\mathbf{Y}_{:,1}^B$, $\mathbf{Y}_{:,2}^B$, and $\mathbf{Y}_{:,3}^B$ are the 3D beamspace data for the receiving side, and the three rows of \mathbf{Y}_B : $\mathbf{Y}_{1,:}^B$, $\mathbf{Y}_{2,:}^B$, and $\mathbf{Y}_{3,:}^B$ are the 3D beamspace data for the transmitting side.

Define

$$\mathbf{C}_r(\theta_1) = \begin{bmatrix} \mathbf{c}_r(\theta_1) & \mathbf{c}_r(\theta_2) \end{bmatrix} = \begin{bmatrix} \mathbf{T}_r^H\mathbf{a}_r(\theta_1) & \mathbf{T}_r^H\mathbf{a}_r(\theta_2) \end{bmatrix} \quad (13)$$

$$\mathbf{C}_t(\theta_1) = \begin{bmatrix} \mathbf{c}_t(\theta_1) & \mathbf{c}_t(\theta_2) \end{bmatrix} = \begin{bmatrix} \mathbf{T}_t^H\mathbf{a}_t(\theta_1) & \mathbf{T}_t^H\mathbf{a}_t(\theta_2) \end{bmatrix} \quad (14)$$

By substituting Equations (11) and (12) into Equation (10), a new form of \mathbf{Y}_B is obtained as

$$\mathbf{Y}_B = \mathbf{C}_r(\theta_1)\boldsymbol{\eta}\mathbf{C}_t^T(\theta_1) + \mathbf{N}_s \quad (15)$$

where

$$\boldsymbol{\eta} = \alpha\sqrt{L} \begin{bmatrix} 1 \\ \varepsilon \end{bmatrix} \begin{bmatrix} 1 & \varepsilon \end{bmatrix} = \alpha\sqrt{L} \begin{bmatrix} 1 & \varepsilon \\ \varepsilon & \varepsilon^2 \end{bmatrix} \quad (16)$$

2.2. Initial Angle Estimation

Given that the BSC algorithm will classify the scene using the multipath coefficient, the solution to the multipath coefficient requires an initial angle estimate. Thus, this subsection describes a method for resolving initial angles with a modest degree of complexity.

For the SF-BML algorithm described in [2,3], the one-dimensional noise subspace is orthogonal to the two-dimensional signal subspace in the eigenvector space of the beamspace sample correlation matrix. SF-BML provides a closed-form solution for angle estimation via this feature. However, as stated in Claim 1 of [26], the closed-form solutions for elevation angle cannot be derived directly using SF-BML for a MIMO radar. The 3D-BMLF algorithm transforms the MIMO radar data into phase array radar data, and then solves the angle with a minimal computational burden. This subsection provides an estimate of the initial elevation angle in accordance with the 3D-BMLF concept.

The 3D beamspace data with the highest power are employed to determine the initial elevation angle estimate. The beamspace data corresponding to the highest power for the receiving side are given as

$$z_{Br} = \begin{cases} \mathbf{Y}_{:,2}^B, & \|\mathbf{Y}_{:,2}^B\|_2 \geq \|\mathbf{Y}_{:,3}^B\|_2 \\ \mathbf{Y}_{:,3}^B, & \text{otherwise} \end{cases} \quad (17)$$

For the sake of analysis, it is assumed that $z_{Br} = \mathbf{Y}_{:,2}^B$ and

$$z_{Br} = \beta \mathbf{C}_r(\theta_1) \begin{bmatrix} 1 \\ \varepsilon \end{bmatrix} + \mathbf{n}_{sr} \quad (18)$$

where $\beta = \alpha \sqrt{\mathbf{L} \mathbf{b}_t^T(\theta_1) \mathbf{a}_t^*(0)}$ is a constant, $\mathbf{n}_{sr} = \mathbf{T}_r^H \mathbf{N}_{s0} \mathbf{a}_t^*(0)$. The ML function of z_{Br} is given as

$$\underset{\theta_1, \theta_2}{\text{Maximize}} z_{Br}^H \mathbf{P}_{Cr}(\theta_1) z_{Br} = \underset{\theta_1, \theta_2}{\text{Minimize}} z_{Br}^H \mathbf{P}_{Cr}^\perp(\theta_1) z_{Br} \quad (19)$$

where $\mathbf{P}_{Cr}^\perp(\theta_1) = \mathbf{I}_3 - \mathbf{P}_{Cr}$, and $\mathbf{P}_{Cr} = \mathbf{C}_r(\theta_1) [\mathbf{C}_r^T(\theta_1) \mathbf{C}_r(\theta_1)]^{-1} \mathbf{C}_r^T(\theta_1)$. Zoltowski et al. [2] and Chen et al. [26] established the closed-form solution for Equation (19) in cases where $h_r \ll R_d$, as

$$\hat{\theta}_r^0 = \arcsin \left[\arctan \left\{ \sqrt{\left[\frac{v_{r2} - 2v_{r1} \cos\left(\frac{\pi}{M_r}\right)}{v_{r2} \cos\left(\frac{2\pi}{M_r}\right) - 2v_{r1} \cos\left(\frac{\pi}{M_r}\right)} \right]^2 - 1} \right\} \frac{\lambda}{2\pi d} \right] \quad (20)$$

where v_{r1}, v_{r2} , and v_{r3} are the elements of \mathbf{v}_r , namely, $\mathbf{v}_r = [v_{r1} \ v_{r2} \ v_{r3}]^T$. \mathbf{v}_r is the eigenvector corresponding to the smallest eigenvalue of

$$R_{br} = \frac{\text{Re}\{z_{Br} z_{Br}^H\} + \tilde{\mathbf{I}}_3 \text{Re}\{z_{Br} z_{Br}^H\} \tilde{\mathbf{I}}_3}{2} \quad (21)$$

where

$$\tilde{\mathbf{I}}_3 = \begin{bmatrix} 0 & 0 & 1 \\ 0 & 1 & 0 \\ 1 & 0 & 0 \end{bmatrix} \quad (22)$$

Next, the beamspace data with the highest power for the transmitting side are given as

$$z_{Bt} = \begin{cases} \mathbf{Y}_{2,:}^B, & \|\mathbf{Y}_{2,:}^B\|_2 \geq \|\mathbf{Y}_{3,:}^B\|_2 \\ \mathbf{Y}_{3,:}^B, & \text{otherwise} \end{cases} \quad (23)$$

For the sake of analysis, it is assumed that $z_{Bt} = \mathbf{Y}_{2,:}^B$ and

$$z_{Bt} = \gamma [1 \ \varepsilon] \mathbf{C}_t^T(\theta_1) + \mathbf{n}_{st} \quad (24)$$

where $\gamma = \alpha \sqrt{\mathbf{L} \mathbf{a}_r^H(0) \mathbf{b}_r(\theta_1)}$ is a constant and $\mathbf{n}_{st} = \mathbf{a}_r^H(0) \mathbf{N}_{s0} \mathbf{T}_t^*$. Similarly, for the cases where $h_r \ll R_d$, $\mathbf{v}_t = [v_{t1} \ v_{t2} \ v_{t3}]^T$ can be obtained as the eigenvector corresponding to the smallest eigenvalue of

$$R_{bt} = \frac{\text{Re}\{z_{Bt} z_{Bt}^H\} + \tilde{\mathbf{I}}_3 \text{Re}\{z_{Bt} z_{Bt}^H\} \tilde{\mathbf{I}}_3}{2} \quad (25)$$

The solution for the target angle based on z_{Bt} can also be obtained by

$$\hat{\theta}_t^0 = \arcsin \left[\arctan \left\{ \sqrt{\left[\frac{v_{t2} - 2v_{t1} \cos\left(\frac{\pi}{M_t}\right)}{v_{t2} \cos\left(\frac{2\pi}{M_t}\right) - 2v_{t1} \cos\left(\frac{\pi}{M_t}\right)} \right]^2 - 1} \right\} \frac{\lambda}{2\pi d} \right] \tag{26}$$

Thus, the initial angle is estimated as

$$\hat{\theta}_1^0 = \frac{\hat{\theta}_t^0 + \hat{\theta}_r^0}{2} \tag{27}$$

2.3. Multipath Coefficient Estimation for Scene Classification

The amplitude of the multipath coefficient can reflect the strength of the multipath component in echo signals. According to [42], the surface reflection coefficient is primarily influenced by working frequency, the type of surface, the signal polarization, and the undulation of the reflection surface. The surface reflection coefficient amplitude (RCA) is greatly affected by polarization and the undulation of the reflection surface. The strong multipath component, i.e., a large surface reflection coefficient amplitude, is typically observed in the case of horizontal polarization and flat terrain. In this scenario, the multipath signal is close to the ideal specular reflection, and the surface reflection coefficient is relatively stable and can be computed accurately. The weak multipath component is most prevalent in the case of vertical polarization or undulating reflection surfaces. In this scenario, it is difficult to identify the actual reflection conditions. The absence of a multipath component generally occurs when obstacles prevent the multipath signal from entering the radar antenna.

In this subsection, the various multipath scenes are classified based on the amplitude of the multipath coefficient. The BPS algorithm estimates the multipath coefficient of the phase radar by eliminating unknown parameters. However, the BPS algorithm is cumbersome for MIMO radar. Thus, a straightforward and effective estimation method is required as an alternative.

The parameter η can be estimated from Equation (15) as follows

$$\eta = C_r^+(\theta_1) Y_B [C_t^T(\theta_1)]^+ - C_r^+(\theta_1) T_r^H N_{s0} T_t^* [C_t^T(\theta_1)]^+ \tag{28}$$

Replacing θ_1 with $\hat{\theta}_1^0$ in Equation (28) and taking into account that noise is independent of the target signals, Equation (28) can be approximated as

$$\eta \approx C_r^+(\hat{\theta}_1^0) Y_B [C_t^T(\hat{\theta}_1^0)]^+ = \begin{bmatrix} \eta_{11} & \eta_{12} \\ \eta_{21} & \eta_{22} \end{bmatrix} \tag{29}$$

Then, ε is estimated from Equations (16) and (29) as follows:

$$\varepsilon = \frac{\eta_{21} + \eta_{22}}{\eta_{11} + \eta_{12}} \tag{30}$$

Again, according to the analysis of RCA in [42], the strength of the multipath component is characterized by the amplitude of the multipath coefficient as

$$\begin{cases} \text{strong,} & |\hat{\varepsilon}| \geq 0.7 \\ \text{weak,} & 0.1 \leq |\hat{\varepsilon}| < 0.7 \\ \text{no,} & |\hat{\varepsilon}| < 0.1 \end{cases} \tag{31}$$

When $|\hat{\varepsilon}|$ is less than 0.1, the very weak multipath component is considered as noise in Equation (31).

2.4. Data Selection for Angle Estimation

To keep the computational complexity of the BSC algorithm low, the algorithm employs an angle-estimation strategy at the transmitter and receiver, which necessitates the creation of appropriate data. The variable δ is specified using a piecewise function as below

$$\delta = \begin{cases} 1, & |\hat{\varepsilon}| \geq 0.1 \\ 0, & |\hat{\varepsilon}| < 0.1 \end{cases} \tag{32}$$

When $\delta = 0$, the signal subspace for the 3D beamspace data is one-dimensional, which means that the eigenvector corresponding to the minimum eigenvalue of the covariance matrix is not orthogonal to the signal subspace. In such cases, the estimations in Equations (20) and (26) are invalid. When $\delta = 0$, the beamspace data are abandoned in the negative angle direction in order to find a one-dimension noise subspace orthogonal to the one-dimension signal subspace in the eigenvector space of the beamspace sample correlation matrix. Equation (12) allows for the expression of 3D and 2D beamspace data as

$$\mathbf{Y}_{B3} = \begin{bmatrix} y_{11} & y_{12} & y_{13} \\ y_{21} & y_{22} & y_{23} \\ y_{31} & y_{32} & y_{33} \end{bmatrix} \tag{33}$$

$$\mathbf{Y}_{B2} = \begin{bmatrix} y_{22} & y_{23} \\ y_{32} & y_{33} \end{bmatrix} \tag{34}$$

During the initial estimation, the beamspace data with the highest power are selected, which corresponds to a certain loss. Although the data of the three beams cannot be coherently accumulated, it is possible to process the data of the three beams incoherently.

The deviation between the target angle and the beam pointing is used to evaluate the gain of the beams on the target signal. Specifically, the gain coefficient for the receiving side is defined as

$$g_r^i = \frac{f_r^i}{\sum_{i=1}^3 f_r^i} \tag{35}$$

$$f_r^i = \frac{\delta + (1 - \delta)(i - 1)^{i-3}}{(\hat{\theta}_r^0 - (i - 2)\theta_r)^2}, i = 1, 2, 3 \tag{36}$$

The gain coefficient for the transmitting side, g_t^i , can also be obtained by $\hat{\theta}_t^0$ and θ_t in the same way as for the receiving side. Then, the fused 3D and 2D beamspace data for receiving and transmitting sides can be obtained as

$$\mathbf{z}_{Br3} = [y_r^1 \quad y_r^2 \quad y_r^3]^T \tag{37}$$

$$\mathbf{z}_{Bt3} = [y_t^1 \quad y_t^2 \quad y_t^3]^T \tag{38}$$

$$\mathbf{z}_{Br2} = [y_r^2 \quad y_r^3]^T \tag{39}$$

$$\mathbf{z}_{Bt2} = [y_t^2 \quad y_t^3]^T \tag{40}$$

where

$$y_r^i = \sum_{j=1}^3 g_r^j y_{ij} \tag{41}$$

$$y_t^j = \sum_{i=1}^3 g_t^i y_{ij} \tag{42}$$

2.5. The Angle Estimation for Transmitting and Receiving Sides

The preceding section transformed the MIMO radar data into phase radar data. The angle-estimation methods corresponding to three cases with distinct multipath components are developed in this subsection.

2.5.1. The Angle Estimation for Strong Multipath Component

When $|\hat{\epsilon}| \geq 0.7$ holds, the surface reflection coefficient can generally be calculated accurately. The BPS algorithm is an excellent candidate angle-estimation method for ideal specular reflection. Similarly to the method described in Section 2.3, a more concise method than the BPS algorithm is developed here, which has the same accuracy as the BPS algorithm.

From Equation (18), it can be inferred that

$$\boldsymbol{\eta}_r = \beta \begin{bmatrix} 1 \\ \epsilon \end{bmatrix} = \mathbf{C}_r^+(\theta_1) \mathbf{z}_{Br} - \mathbf{C}_r^+(\theta_1) \mathbf{n}_{sr} \tag{43}$$

Replacing θ_1 with $\hat{\theta}_1^0$ in Equation (43), and taking into account that noise is independent of the target signals, Equation (43) can be approximated as

$$\boldsymbol{\eta}_r \approx \mathbf{C}_r^+(\hat{\theta}_1^0) \mathbf{z}_{Br} = \begin{bmatrix} \eta_{r1} \\ \eta_{r2} \end{bmatrix} \tag{44}$$

Then, the multipath coefficient is estimated for the receiving side as

$$\hat{\epsilon}_r = \frac{\eta_{r1}}{\eta_{r2}} \tag{45}$$

The corresponding multipath phase estimate reads as

$$\hat{\psi}_{r0} = \arctan(\text{Im}\{\hat{\epsilon}_r\} / \text{Re}\{\hat{\epsilon}_r\}) \tag{46}$$

Due to the periodic nature of the phase, the estimation of $\hat{\psi}_{r0}$ may be ambiguous. The multipath phase corresponding to the initial estimate $\hat{\theta}_1^0$ is

$$\psi(\hat{\theta}_1^0) = \phi_\rho - \frac{4\pi h_r (\sin \hat{\theta}_1^0 + h_r / R_d)}{\lambda} \tag{47}$$

The approximate value of the multipath phase is known from Equation (47), which can be used to correct the estimated value. The difference between the approximate and true values is approximately an integer multiple of 2π . Thus, the correct estimation of the multipath phase is obtained as

$$\hat{\psi}_r = \hat{\psi}_{r0} + \left\langle \frac{\psi(\hat{\theta}_1^0) - \hat{\psi}_{r0}}{2\pi} \right\rangle 2\pi \tag{48}$$

From Equation (7), the angle is estimated for receiving side as

$$\hat{\theta}_{r1} = \arcsin \left\{ \frac{\lambda [\phi_\rho - \hat{\psi}_r]}{4\pi h_r} - \frac{h_r}{R_d} \right\} \tag{49}$$

To obtain high accuracy in angle estimation, the estimation process is performed twice, with the angle estimate in the first instance replacing $\hat{\theta}_1^0$ in the second instance.

In the same way, the results for the transmitting side can be derived as

$$\boldsymbol{\eta}_t = \gamma \begin{bmatrix} 1 \\ \epsilon \end{bmatrix} \approx \mathbf{z}_{Bt} [\mathbf{C}_t^T(\hat{\theta}_1^0)]^+ = \begin{bmatrix} \eta_{t1} \\ \eta_{t2} \end{bmatrix} \tag{50}$$

$$\hat{\epsilon}_t = \frac{\eta_{t1}}{\eta_{t2}} \tag{51}$$

$$\hat{\psi}_{t0} = \arctan\left(\frac{\text{Im}\{\hat{\epsilon}_t\}}{\text{Re}\{\hat{\epsilon}_t\}}\right) \tag{52}$$

$$\hat{\psi}_t = \hat{\psi}_{t0} + \left\langle \frac{\psi(\hat{\theta}_1^0) - \hat{\psi}_{t0}}{2\pi} \right\rangle 2\pi \tag{53}$$

$$\hat{\theta}_{t1} = \arcsin\left\{ \frac{\lambda[\phi_\rho - \hat{\psi}_t]}{4\pi h_r} - \frac{h_r}{R_d} \right\} \tag{54}$$

2.5.2. The Angle Estimation for Weak Multipath Component

When $0.1 \leq |\hat{\epsilon}| < 0.7$ holds, the actual reflection conditions are generally unstable and difficult to determine precisely because of vertical polarization or an undulating reflection surface. The angle-estimation process outlined in Section 2.2 is therefore taken into account. Based on the beamspace data of Equations (37) and (38), the angle estimates $\hat{\theta}_{r2}$ and $\hat{\theta}_{t2}$ can be obtained by Equations (20) and (26).

2.5.3. The Angle Estimation for no Multipath Component

When $|\hat{\epsilon}| < 0.1$, the weak multipath component is treated as noise. According to the solution method for 2D beamspace data described in [3], the closed-form solution of the target angle can be obtained using the eigenvector corresponding to the smallest eigenvalue of the 2D beamspace sample correlation matrix.

Based on Equations (39) and (40), the 2D beamspace sample correlation matrices for receiving and transmitting sides are given as

$$\mathbf{R}_{Br2} = \text{Re}\left\{ \mathbf{z}_{Br2} \mathbf{z}_{Br2}^H \right\} \tag{55}$$

$$\mathbf{R}_{Bt2} = \text{Re}\left\{ \mathbf{z}_{Bt2} \mathbf{z}_{Bt2}^H \right\} \tag{56}$$

Let $\mathbf{p}_r = [p_{r1} \ p_{r2}]^T$ and $\mathbf{p}_t = [p_{t1} \ p_{t2}]^T$ be the eigenvectors corresponding to the smallest eigenvalue of \mathbf{R}_{Br2} and \mathbf{R}_{Bt2} . The closed-form solutions of the target angle for 2D beamspace data can be derived as [3]

$$\hat{\theta}_{r2} = \arcsin\left\{ \frac{\lambda}{2d} \left\{ \frac{1}{M_r} + \frac{2}{\pi} \arctan\left\{ \left[\frac{p_{r1} + p_{r2}}{p_{r1} - p_{r2}} \right] \tan\left(\frac{\pi}{2M_r}\right) \right\} \right\} \right\} \tag{57}$$

$$\hat{\theta}_{t2} = \arcsin\left\{ \frac{\lambda}{2d} \left\{ \frac{1}{M_t} + \frac{2}{\pi} \arctan\left\{ \left[\frac{p_{t1} + p_{t2}}{p_{t1} - p_{t2}} \right] \tan\left(\frac{\pi}{2M_t}\right) \right\} \right\} \right\} \tag{58}$$

Then, the angle estimation for the receiving and transmitting sides can be expressed as

$$\hat{\theta}_r = [\hat{\theta}_{r1} \ \hat{\theta}_{r2} \ \hat{\theta}_{r3}] \boldsymbol{\zeta} \tag{59}$$

$$\hat{\theta}_t = [\hat{\theta}_{t1} \ \hat{\theta}_{t2} \ \hat{\theta}_{t3}] \boldsymbol{\zeta} \tag{60}$$

where

$$\boldsymbol{\zeta} = \begin{cases} \begin{bmatrix} 1 & 0 & 0 \end{bmatrix}^T, & |\hat{\epsilon}| \geq 0.7 \\ \begin{bmatrix} 0 & 1 & 0 \end{bmatrix}^T, & 0.1 \leq |\hat{\epsilon}| < 0.7 \\ \begin{bmatrix} 0 & 0 & 1 \end{bmatrix}^T, & |\hat{\epsilon}| < 0.1 \end{cases} \tag{61}$$

2.6. Fusion of Two Angle Estimations

We had two angle estimations above: one for the receiving side and one for the transmitting side. To attain a high estimation accuracy, it is necessary to identify two appropriate weights w_r and w_t to fuse $\hat{\theta}_r$ and $\hat{\theta}_t$ as

$$\hat{\theta}_1 = w_r \hat{\theta}_r + w_t \hat{\theta}_t \tag{62}$$

According to the criterion of minimizing the MSE, Chen et al. [26] determined the optimal weights w_r and w_t as

$$w_r = \frac{\sigma_{\hat{\theta}_t}^2}{\sigma_{\hat{\theta}_t}^2 + \sigma_{\hat{\theta}_r}^2} \tag{63}$$

$$w_t = \frac{\sigma_{\hat{\theta}_r}^2}{\sigma_{\hat{\theta}_t}^2 + \sigma_{\hat{\theta}_r}^2} = 1 - w_r \tag{64}$$

where $\sigma_{\hat{\theta}_r}^2$ and $\sigma_{\hat{\theta}_t}^2$ are the MSE of $\hat{\theta}_r$ and $\hat{\theta}_t$. This required the determination of the MSE.

For $|\hat{\epsilon}| \geq 0.7$, the estimation is performed based on the refined signal model, which assumes that the surface reflection coefficient and the geometric information between θ_1 and θ_2 are known. As demonstrated in [43,44], the MSE of $\hat{\theta}_r$ and $\hat{\theta}_t$ utilizing the refined signal model for 3D beamspace data can be deduced as

$$\sigma_{\hat{\theta}_r}^2 = \frac{\sigma_r^2}{2|\beta|^2 \text{Re}(\mathbf{d}_r^H(\theta_1) \mathbf{P}_{br}^\perp \mathbf{d}_r(\theta_1))} \tag{65}$$

$$\sigma_{\hat{\theta}_t}^2 = \frac{\sigma_t^2}{2|\gamma|^2 \text{Re}(\mathbf{d}_t^H(\theta_1) \mathbf{P}_{bt}^\perp \mathbf{d}_t(\theta_1))} \tag{66}$$

where σ_r^2 and σ_t^2 are the noise power of a single beam, respectively. $\mathbf{d}_r(\theta_i) = \mathbf{T}_r^H \frac{\partial}{\partial \theta_i} \mathbf{a}_r(\theta_i) i = 1, 2$, $\mathbf{d}_t(\theta_i) = \mathbf{T}_t^H \frac{\partial}{\partial \theta_i} \mathbf{a}_t(\theta_i) i = 1, 2$, $\mathbf{P}_{br}^\perp = \mathbf{I} - \mathbf{P}_{br}$, $\mathbf{P}_{br} = \mathbf{b}_{Br}(\theta_1) [\mathbf{b}_{Br}^T(\theta_1) \mathbf{b}_{Br}(\theta_1)]^{-1} \mathbf{b}_{Br}^T(\theta_1)$, $\mathbf{P}_{bt}^\perp = \mathbf{I} - \mathbf{P}_{bt}$, $\mathbf{P}_{bt} = \mathbf{b}_{Bt}(\theta_1) [\mathbf{b}_{Bt}^T(\theta_1) \mathbf{b}_{Bt}(\theta_1)]^{-1} \mathbf{b}_{Bt}^T(\theta_1)$. Then, the corresponding weights are obtained as

$$w_{r1} = \frac{\sigma_{\hat{\theta}_t}^2}{\sigma_{\hat{\theta}_t}^2 + \sigma_{\hat{\theta}_r}^2} = \frac{1}{1 + \frac{M_r \|\mathbf{b}_r(\theta_1)\|_2^2 \text{Re}(\mathbf{d}_t^H(\theta_1) \mathbf{P}_{bt}^\perp \mathbf{d}_t(\theta_1))}{M_t \|\mathbf{b}_t(\theta_1)\|_2^2 \text{Re}(\mathbf{d}_r^H(\theta_1) \mathbf{P}_{br}^\perp \mathbf{d}_r(\theta_1))}} = \frac{1}{1 + w_{01}} \tag{67}$$

where

$$w_{01} = \frac{M_r \|\mathbf{b}_r(\theta_1)\|_2^2 \text{Re}(\mathbf{d}_t^H(\theta_1) \mathbf{P}_{bt}^\perp \mathbf{d}_t(\theta_1))}{M_t \|\mathbf{b}_t(\theta_1)\|_2^2 \text{Re}(\mathbf{d}_r^H(\theta_1) \mathbf{P}_{br}^\perp \mathbf{d}_r(\theta_1))} \tag{68}$$

For $0.1 \leq |\hat{\epsilon}| < 0.7$, the geometric information between θ_1 and θ_2 is assumed to be given. As demonstrated in [26,44], the MSE of $\hat{\theta}_r$ and $\hat{\theta}_t$ utilizing the geometric information for 3D beamspace data can be obtained as

$$\sigma_{\hat{\theta}_r}^2 = \frac{\sigma_r^2}{2|\beta|^2 \text{Re}(\mathbf{\Gamma}^H \mathbf{D}_r^H \mathbf{P}_{Cr}^\perp \mathbf{D}_r \mathbf{\Gamma})} \tag{69}$$

$$\sigma_{\hat{\theta}_t}^2 = \frac{\sigma_t^2}{2|\gamma|^2 \text{Re}(\mathbf{\Gamma}^H \mathbf{D}_t^H \mathbf{P}_{Ct}^\perp \mathbf{D}_t \mathbf{\Gamma})} \tag{70}$$

where $\Gamma = [1 \ \varepsilon]^T$, $D_r = [d_r(\theta_1), d_r(\theta_2)]$, $D_t = [d_t(\theta_1), d_t(\theta_2)]$, $P_{Ct}^\perp = I_3 - P_{Ct}$, $P_{Ct} = C_t(\theta_1) [C_t^T(\theta_1) C_t(\theta_1)]^{-1} C_t^T(\theta_1)$. Then, the corresponding weights are derived as

$$w_{r2} = \frac{\sigma_{\hat{\theta}t2}^2}{\sigma_{\hat{\theta}t2}^2 + \sigma_{\hat{\theta}r2}^2} = \frac{1}{1 + \frac{M_r \|b_r(\theta_1)\|_2^2 \text{Re}(\Gamma^H D_r^H P_{Ct}^\perp D_t \Gamma)}{M_t \|b_t(\theta_1)\|_2^2 \text{Re}(\Gamma^H D_r^H P_{Cr}^\perp D_r \Gamma)}} = \frac{1}{1 + w_{02}} \tag{71}$$

where

$$w_{02} = \frac{M_r \|b_r(\theta_1)\|_2^2 \text{Re}(\Gamma^H D_r^H P_{Ct}^\perp D_t \Gamma)}{M_t \|b_t(\theta_1)\|_2^2 \text{Re}(\Gamma^H D_r^H P_{Cr}^\perp D_r \Gamma)} \tag{72}$$

For $|\hat{\varepsilon}| < 0.1$ when the beamspace data in the negative angle direction are abandoned, the MSE of $\hat{\theta}_r$ and $\hat{\theta}_t$ for 2D beamspace data can be estimated as [43]

$$\sigma_{\hat{\theta}r2}^2 = \frac{2/3\sigma_r^2}{2|\beta|^2 \text{Re}(d_r^H(\theta_1) P_{Dr}^\perp d_r(\theta_1))} \tag{73}$$

$$\sigma_{\hat{\theta}t2}^2 = \frac{2/3\sigma_t^2}{2|\beta|^2 \text{Re}(d_t^H(\theta_1) P_{Dt}^\perp d_t(\theta_1))} \tag{74}$$

where $P_{Dr}^\perp = I_2 - P_{Dr}$, $P_{Dt}^\perp = I_2 - P_{Dt}$, $P_{Dr} = T_{r2}^H a_r(\theta_1) [a_r^T(\theta_1) T_{r2}^* T_{r2}^H a_r(\theta_1)]^{-1} a_r^T(\theta_1) T_{r2}^*$, $P_{Dt} = T_{t2}^H a_t(\theta_1) [a_t^T(\theta_1) T_{t2}^* T_{t2}^H a_t(\theta_1)]^{-1} a_t^T(\theta_1) T_{t2}^*$. In the same way, the corresponding weights can be obtained as

$$w_{r3} = \frac{1}{1 + w_{03}} \tag{75}$$

$$w_{03} = \frac{M_r^2 \text{Re}(d_t^H(\theta_1) P_{Dt}^\perp d_t(\theta_1))}{M_t^2 \text{Re}(d_r^H(\theta_1) P_{Dr}^\perp d_r(\theta_1))} \tag{76}$$

Then, by substituting $\hat{\theta}_r$ and $\hat{\theta}_t$ for θ_1 , and $\hat{\varepsilon}_r$ and $\hat{\varepsilon}_t$ for ε on the receiving and transmitting sides, the weights w_r and w_t are obtained. To sum up, the weight w_r can then be expressed as

$$w_r = [w_{r1} \ w_{r2} \ w_{r3}] \xi = \frac{1}{1 + [w_{01} \ w_{02} \ w_{03}] \xi} \tag{77}$$

with $w_t = 1 - w_r$, the final estimation of the target angle reads as

$$\hat{\theta}_1 = w_r \hat{\theta}_r + w_t \hat{\theta}_t = \frac{\hat{\theta}_r + [w_{01} \ w_{02} \ w_{03}] \xi \hat{\theta}_t}{1 + [w_{01} \ w_{02} \ w_{03}] \xi} \tag{78}$$

It is worth noting that the closed-form solutions for the weak multipath component and the absence of a multipath component are constrained by the structure of the uniform linear array. Furthermore, the proposed method is only applicable to the scene of a single target in a multipath environment. In a multiple target scenario, multiple targets require separation in the range, Doppler, and angle dimensions through signal processing. The flow chart of the BSC algorithm is summarized in Figure 2.

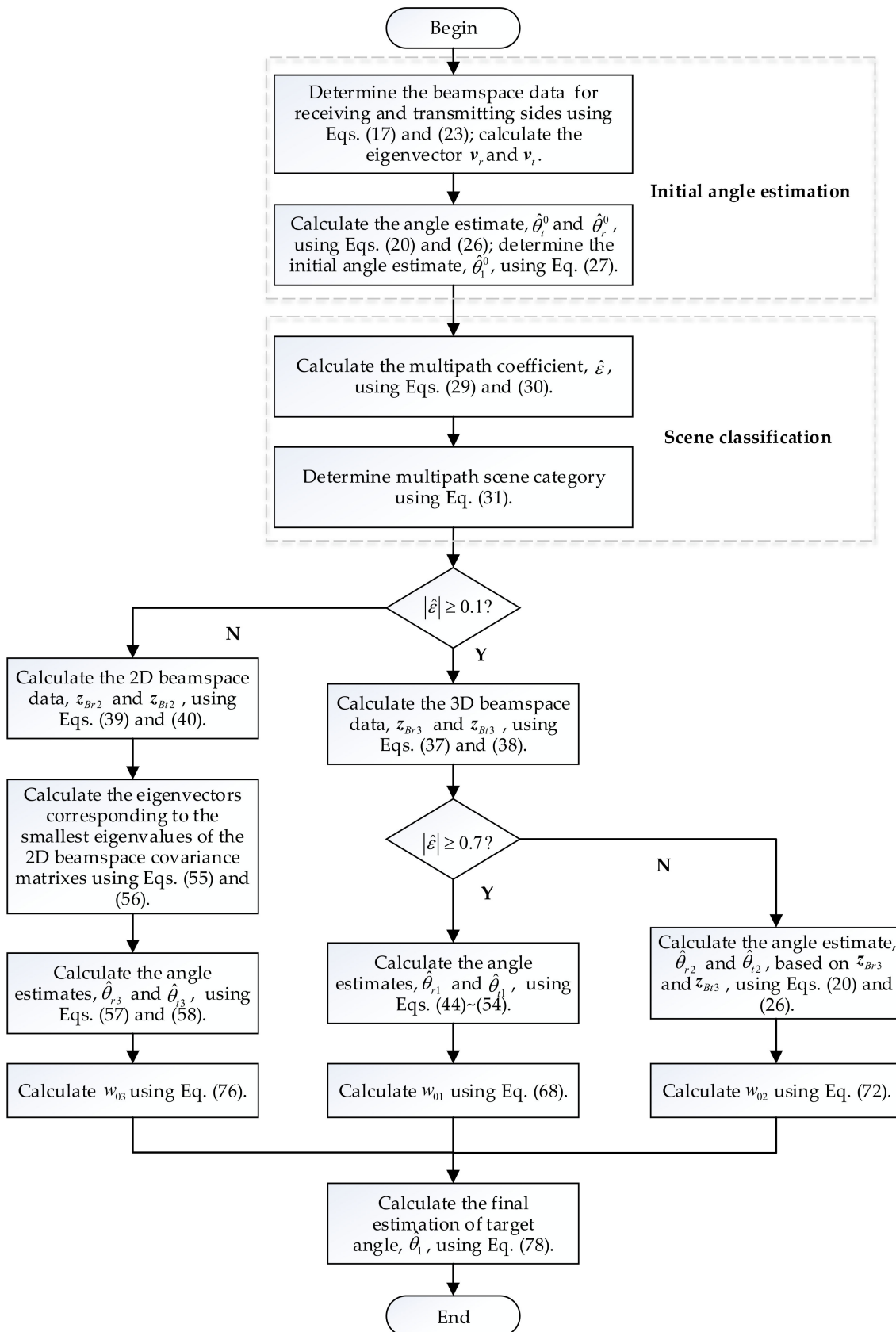


Figure 2. The flow chart of the BSC algorithm.

2.7. The Simplified Angle-Estimation Method

Furthermore, in the case of $M_r = M_t$, the beamspace data for the receiving and transmitting sides are identical to the two samples of the same signal. Thus, the beamspace data for both the receiving and transmitting sides can be added directly. Then, the solution of the simplified BSC algorithm for target angle can be achieved directly without requiring a fusion process.

3. Results

This section discusses the angle-estimation performances of the BIML, 3D-BMLF, and BSC algorithms, as well as the CRB for refined signal models [5] through computer simulations.

Consider a narrowband collocated MIMO radar equipped with a uniform linear array. The linear array is mounted vertically in the horizontal plane. The input parameters are set to $\lambda = 0.3$ m, $d = 0.15$ m, $h_r = 1.2$ m, $M_t = M_r = 12$, and $R_d = 50$ km. The radar transmits signals with an orthogonal waveform and a bandwidth of 1 MHz. A pulse contains 800 sample points, and the signal envelope follows a Swerling 0 nonfluctuation model. Other simulation parameters are discussed in further detail below. The number of Monte Carlo realizations is set to 500 in each of these simulations. Next, the SNR is defined as

$$SNR = \frac{M_t M_r |\alpha|^2}{\sigma_n^2} \tag{79}$$

Firstly, the RMSEs of the target angle for each of the three algorithms are shown against the target angle in a flat reflector scene. For $\rho = 0.9 \exp(j\pi)$ and SNR = 15 dB, the RMSE of the target angle corresponding to the three algorithms is plotted against the angle and the CRB in Figure 3. The BSC algorithm outperforms the BIML and 3D-BMLF algorithms, especially in high-angle areas, and the BSC algorithm is closer to the CRB than others. When the angle is small, the RMSE of the three algorithms is greater. In addition, the RMSE fluctuates more significantly for BIML and 3D-BMLF.

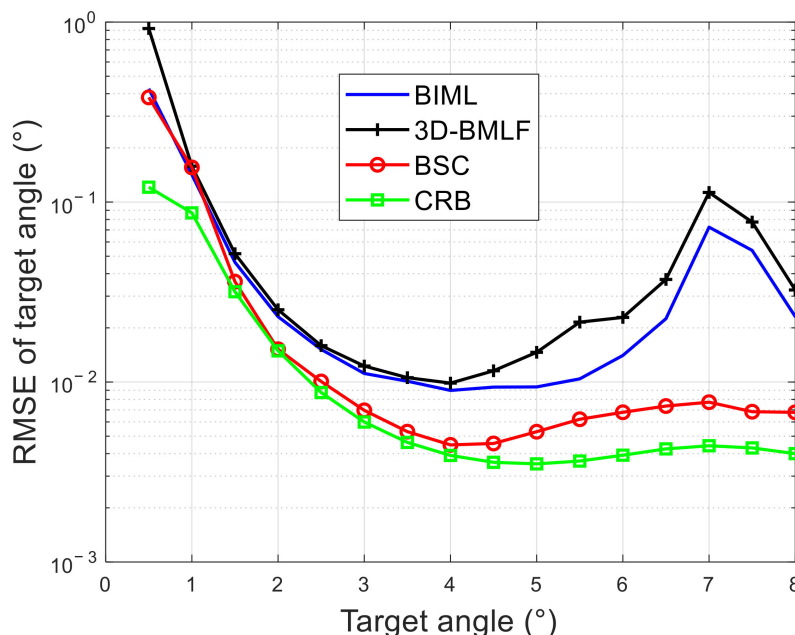


Figure 3. The RMSEs of the target angle for the three algorithms against the angle.

Secondly, the influence of the RCA on the estimation accuracy is investigated. Assuming $\theta_1 = 1.5^\circ$, SNR = 15 dB, and $\rho = |\rho| \exp(j\pi)$, the RMSEs of the target angle for the three algorithms are plotted against the RCA in Figure 4, where the RCA = 0 indicates that no multipath signal exists in the target echo. The estimation error of the BIML and

3D-BMLF algorithms diminishes as the RCA grows. The BSC algorithm achieves the lowest estimation error when the RCA is large than 0.7 or less than 0.1. When the RCA is small but greater than 0.1, the BSC algorithm performs identically to the 3D-BMLF algorithms in terms of estimation accuracy.

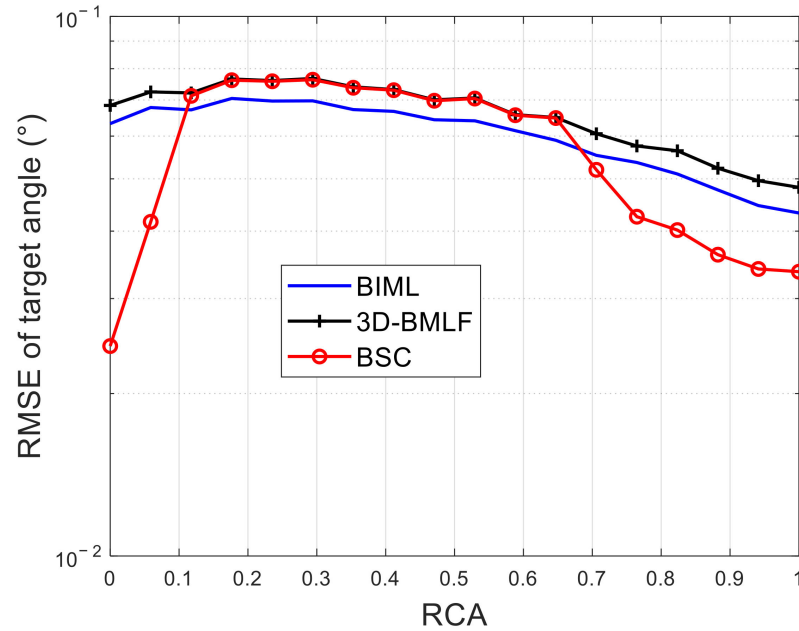


Figure 4. The RMSEs of the target angle for the three algorithms against the RCA.

Thirdly, the RMSE of the target angle for the three algorithms is shown against SNR. Assuming $\theta_1 = 1.5^\circ$ and $\rho = 0.9 \exp(j\pi)$, the RMSEs of the target angle for the three algorithms are shown against SNR in Figure 5. As the SNR increases, the estimation error of the three algorithms reduces. The RMSE of the BSC algorithm is closer to the CRB and is lower than that of the other algorithms. The RMSE of the target angle for the BSC algorithm and the simplified BSC algorithm are plotted against SNR in Figure 6. As observed, the BSC algorithm performs identically to the simplified BSC algorithm in cases where $M_r = M_t$.

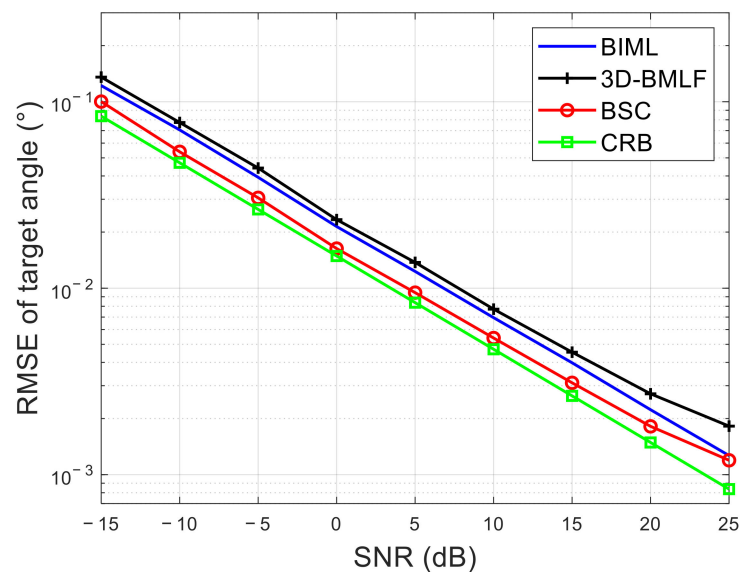


Figure 5. The RMSEs of the target angle for the three algorithms against the SNR.

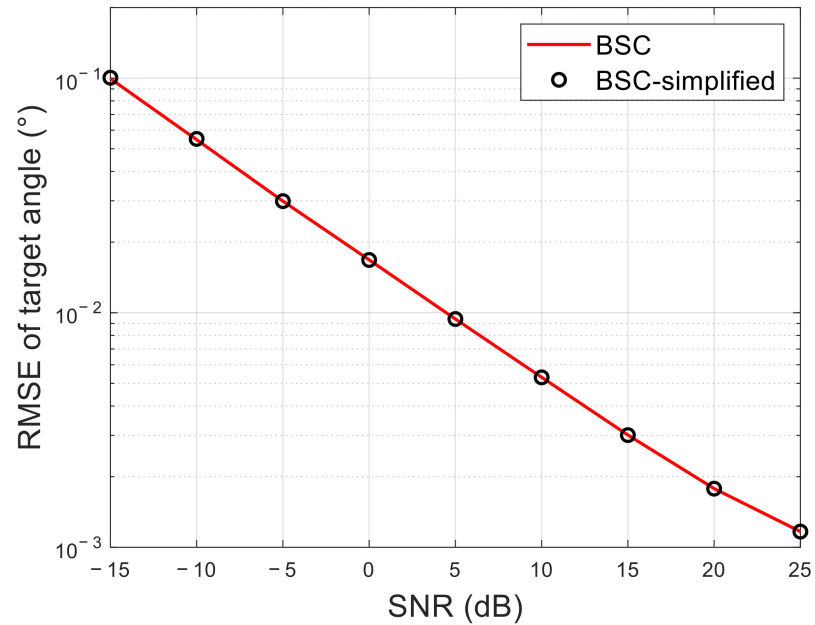


Figure 6. The RMSEs of the target angle for the BSC and simplified BSC algorithms against the SNR.

Fourthly, the RMSE of the target angle for the BSC algorithm under different noise types is shown against the angle. For SNR = 15 dB and $\rho = 0.9 \exp(j\pi)$, Figure 7 shows the RMSE of the target angle for the BSC algorithm against the angle, where the three noise types are Gaussian white noise with a mean value of zero, Gaussian white noise with a mean value of 0.1, and Gaussian colored noise with a mean value of zero, denoted by GW-0, GW-1, and GC, respectively. As can be observed, the BSC algorithm performs differently under various noise types. The estimation accuracy under colored noise is inferior to the estimation accuracy under white noise.

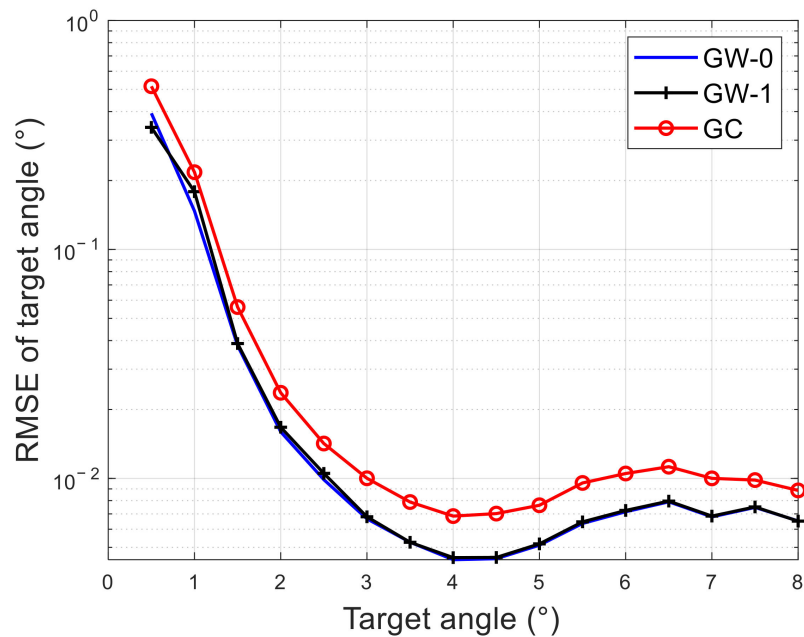


Figure 7. The RMSEs of the target angle for the BSC algorithm under different noise types against the angle.

Fifthly, the influence of the target distance error and the antenna center height error on the accuracy is investigated for the BIML, 3D-BMLF, and BSC algorithms. It is assumed that $\theta_1 = 1.5^\circ$ and $\text{SNR} = 15$ dB. For $\rho = 0.9 \exp(j\pi)$, the RMSEs of the target angle for the three algorithms are plotted against the target distance error in Figure 8. For $\rho = 0.6 \exp(j\pi)$, the RMSEs of the target angle for the three algorithms are illustrated against antenna center height error in Figure 9. As can be observed, the influence of target distance and antenna center height errors on the accuracy of these three algorithms is negligible.

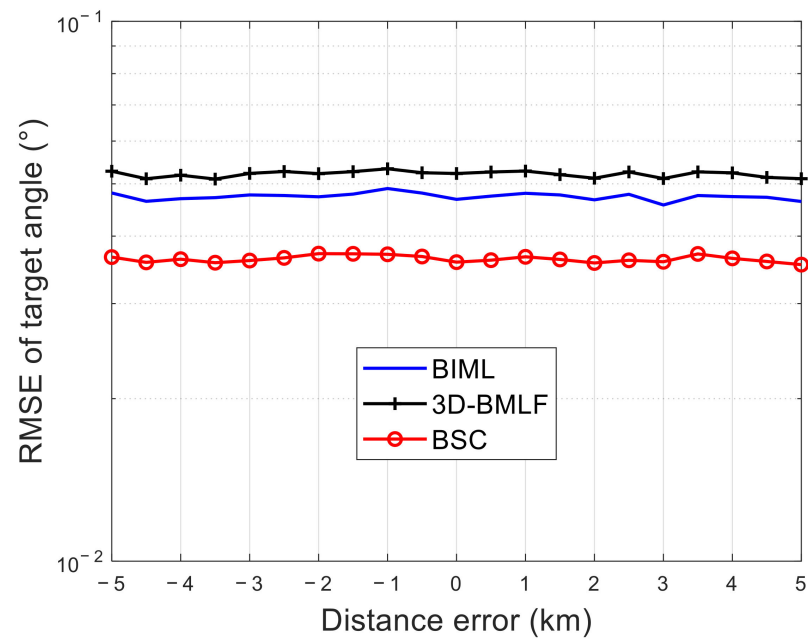


Figure 8. The RMSEs of the target angle for the three algorithms against the target distance error.

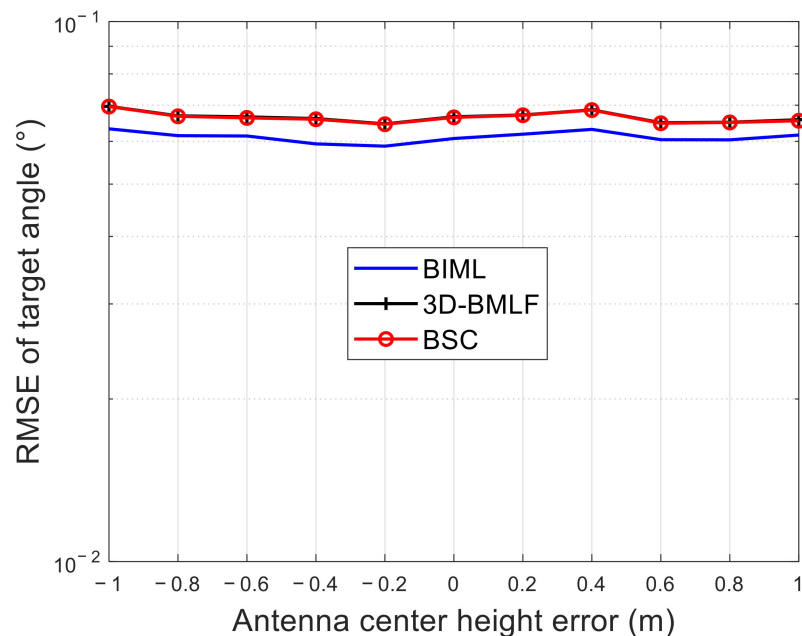


Figure 9. The RMSEs of the target angle for the three algorithms against the antenna center height error.

4. Discussion

4.1. Estimation Accuracy Analysis

The RMSEs of the target angle for each of the three algorithms are plotted against the target angle in a flat reflector scene in Figure 3. The BSC algorithm identifies the ideal scene according to the amplitude of the multipath coefficient and then utilizes the reflection coefficient information. The BIML and 3D-BMLF algorithms suffer from a mismatch problem for composite steering vectors caused by the unused reflection coefficient [5], resulting in a substantial fluctuation in the RMSE variation. When the angle is small, the direct and multipath signals cancel each other, reducing the effective signal power [5]. In addition, although the BSC algorithm separates the transmitting and receiving sides to reduce the computational complexity, it does not take advantage of the aperture expansion of MIMO radar, resulting in estimation accuracy that is insufficient to meet the CRB.

Figure 4 shows the influence of the RCA on the estimation accuracy. The effective signal power increases as the RCA increases. However, estimation accuracy is not solely determined by the effective signal power. In the absence of a multipath scene, the low angle problem is degraded to the angle estimation of a single source. With the strong multipath scene, it is possible to dramatically enhance estimation accuracy by utilizing as much information as possible. When the RCA is large, the BSC algorithm first identifies the ideal scene using the amplitude of the multipath coefficient and then performs angle estimation using the reflection coefficient information; when the RCA is less than 0.1, the BSC algorithm identifies the no-multipath scene and provides an appropriate scheme for estimation. As a result, the BSC algorithm achieves a higher estimation accuracy than other algorithms. When the RCA is small but greater than 0.1, the BSC algorithm identifies the weak multipath scene without relying on information pertaining to reflection coefficients.

The RMSEs of the target angle for the three algorithms are plotted against the SNR in Figure 5. When the SNR is greater than 20 dB, the estimation error of the BSC and 3D-BMLF algorithms is reduced more slowly, as both methods have approximate errors when computing the closed-form solution. When the SNR is large, the influence of approximate errors may outweigh the impact of noise. However, when the SNR exceeds 20 dB, the estimation error is negligible. To achieve such low error with the search-based BIML algorithm, the angle search interval must be less than 0.005° , which is generally unacceptable in engineering applications.

Figures 7–9 illustrate the performance of the BSC algorithm under various noise type, target distance error, and antenna center height error conditions. Under identical SNR and noise distribution conditions, the noise mean does not affect the estimation accuracy of the BSC algorithm, but colored noise will significantly reduce the estimation accuracy. Additionally, although these three algorithms make use of information on the distance and antenna center height throughout the estimation process, the error has minimal effect on the accuracy.

A limitation of this study is that the actual verification cannot be implemented at the moment due to objective reasons. Once it becomes feasible in the future, this experiment will be carried out completely. Additionally, the BSC algorithm is constrained by the structure of the uniform linear array. Therefore, a method independent of the array structure is worth investigating.

4.2. Computational Complexity Analysis

In this subsection, the computational complexity of the BIML, 3D-BMLF, and BSC algorithms is investigated after a matched filter. The number of spectral search grids for the BIML algorithm is P , and the number of beams is $Q = Q_t = Q_r$. The transmit beamformer and receive beamformer were calculated in advance.

The BIML algorithm mainly involves converting the search vector from element space to beamspace and calculating the cost function in the beamspace. The computational complexity of the BIML algorithm is $O(M_t Q + M_r Q + P Q^4)$. The 3D-BMLF algorithm is

primarily concerned with calculating the eigenvectors and weights, and the corresponding computational complexity of the 3D-BMLF algorithm is $O(Q^3 + QM_r + QM_t)$.

The BSC algorithm mainly contains the computation of the initial estimation, the multipath coefficient estimation, the angle estimation for the transmitting and receiving sides, and the fusion. The computational complexity of these four parts of the BSC algorithm is summarized in Table 2. As a result, the computational complexity of the BSC algorithm is determined as $O(Q^3 + QM_r + QM_t)$.

Table 2. Computational complexity of the BSC algorithm.

Computing Procedure	Computational Complexity
The initial estimation	$O(Q^3 + QM_r + QM_t)$
The multipath coefficient estimation	$O(Q^3 + QM_r + QM_t)$
The angle estimation for two sides	$O(Q^3 + QM_r + QM_t)$
The fusion	$O(QM_r + QM_t)$

The computational complexity of these three algorithms is summarized in Table 3. The computational complexity of the BSC algorithm is comparable to that of the 3D-BMLF algorithm, and is obviously less than that of BIML. When combined with prior accuracy estimation, the BSC algorithm becomes more desirable for engineering applications.

Table 3. Computational complexity of the three algorithms.

Algorithms	Computational Complexity
BIML	$O(PQ^4 + QM_r + QM_t)$
3D-BMLF	$O(Q^3 + QM_r + QM_t)$
BSC	$O(Q^3 + QM_r + QM_t)$

5. Conclusions

This paper addresses the problem of beamspace low-angle estimation in MIMO radar. The proposed BSC algorithm solves an initial estimate and the multipath coefficient using 3D beamspace data, constructs the appropriate beamspace data for transmitting and receiving sides, provides three estimation schemes for various multipath scenes, and fuses the estimates for two sides. Although the BSC algorithm does not thoroughly exploit the aperture expansion advantage of MIMO radar, the proposed method achieves high estimation accuracy at a reasonable computational burden. The simulation results and theoretical analysis indicate that the proposed method is more suitable for engineering applications.

Author Contributions: Conceptualization, S.C.; methodology, S.C.; software, S.C., Y.H. and B.N.; validation, S.C.; formal analysis, S.C.; investigation, S.C., Y.H. and B.N.; resources, S.C. and Y.Z.; data curation, S.C., Y.Z. and Y.H.; writing—original draft preparation, S.C.; writing—review and editing, Y.Z., Y.H. and B.N.; visualization, S.C., Y.H. and B.N.; supervision, Y.Z.; project administration, Y.Z.; funding acquisition, Y.Z. All authors have read and agreed to the published version of the manuscript.

Funding: This research was partially supported by the Fund for Foreign Scholars in University Research and Teaching Programs (the 111 Project), grant number B18039.

Data Availability Statement: Not applicable.

Conflicts of Interest: The authors declare no conflict of interest.

References

1. Barton, D.K. Low-angle radar tracking. *IEEE Proc.* **1974**, *62*, 687–704. [\[CrossRef\]](#)
2. Zoltowski, M.D.; Lee, T.-S. Maximum likelihood based sensor array signal processing in the beamspace domain for low angle radar tracking. *IEEE Trans. Signal Process.* **1991**, *39*, 656–671. [\[CrossRef\]](#)
3. Zoltowski, M.D.; Lee, T.-S. Beamspace ML bearing estimation incorporating low-angle geometry. *IEEE Trans. Aerosp. Electron. Syst.* **1991**, *27*, 441–458. [\[CrossRef\]](#)
4. Zhu, Y.; Zhao, Y.; Shui, P. Low-angle target tracking using frequency-agile refined maximum likelihood algorithm. *IET Radar Sonar Navig.* **2016**, *11*, 491–497. [\[CrossRef\]](#)
5. Tan, J.; Nie, Z. Cramer-Rao bound of low angle estimation for VHF monostatic MIMO radar. In Proceedings of the 2018 IEEE Radar Conference, Oklahoma City, OK, USA, 23–27 April 2018; pp. 158–163. [\[CrossRef\]](#)
6. Xu, L.; Jian, L.; Stoica, P. Adaptive Techniques for MIMO Radar. In Proceedings of the Fourth IEEE Workshop on Sensor Array and Multichannel Processing, Waltham, MA, USA, 12–14 July 2006; pp. 258–262. [\[CrossRef\]](#)
7. Bekkerman, I.; Tabrikian, J. Target Detection and Localization Using MIMO Radars and Sonars. *IEEE Trans. Signal Process.* **2006**, *54*, 3873–3883. [\[CrossRef\]](#)
8. Shi, J.; Hu, G.; Zong, B.; Chen, M. DOA Estimation Using Multipath Echo Power for MIMO Radar in Low-Grazing Angle. *IEEE Sens. J.* **2016**, *16*, 6087–6094. [\[CrossRef\]](#)
9. Si, Q.; Zhang, Y.D.; Amin, M.G. Generalized Coprime Array Configurations for Direction-of-Arrival Estimation. *IEEE Trans. Signal Process.* **2015**, *63*, 1377–1390. [\[CrossRef\]](#)
10. Jian, L.; Stoica, P. MIMO Radar with Colocated Antennas. *IEEE Signal Process. Mag.* **2007**, *24*, 106–114. [\[CrossRef\]](#)
11. Shi, J.; Wen, F.; Liu, T. Nested MIMO Radar: Coarrays, Tensor Modeling, and Angle Estimation. *IEEE Trans. Aerosp. Electron. Syst.* **2021**, *57*, 573–585. [\[CrossRef\]](#)
12. Sen, S.; Nehorai, A. OFDM MIMO Radar with Mutual-Information Waveform Design for Low-Grazing Angle Tracking. *IEEE Trans. Signal Process.* **2010**, *58*, 3152–3162. [\[CrossRef\]](#)
13. Zoltowski, M.D.; Kautz, G.M.; Silverstein, S.D. Beamspace Root-MUSIC. *IEEE Trans. Signal Process.* **1993**, *41*, 344–364. [\[CrossRef\]](#)
14. Xu, B.; Zhao, Y. Transmit beamspace-based DOD and DOA estimation method for bistatic MIMO radar. *Signal Process.* **2019**, *157*, 88–96. [\[CrossRef\]](#)
15. Liu, Y.; Hou, L.; Shen, Q.; Lv, C.; Qiu, T. Beamspace U-ESPRIT DOA Estimation Algorithm of Coherently Distributed Sources in Massive MIMO Systems. In Proceedings of the 12th International Conference on Advanced Computational Intelligence (ICACI), Dali, China, 14–16 August 2020. [\[CrossRef\]](#)
16. Yang, R.; Gray, D.; Al-Ashwal, W. Estimation of the DOAs of Coherent Signals in Beam Space Processing for Phased Arrays. In Proceedings of the 2018 International Conference on Radar (RADAR), Brisbane, Australia, 27–31 August 2018; pp. 1–5. [\[CrossRef\]](#)
17. Gao, X.; Dai, L.; Han, S.F.; Chih-Lin, I.; Wang, X. Reliable Beamspace Channel Estimation for Millimeter-Wave Massive MIMO Systems with Lens Antenna Array. *IEEE Trans. Wirel. Commun.* **2017**, *16*, 6010–6021. [\[CrossRef\]](#)
18. Wang, S.; Cao, Y.; Su, H.; Wang, Y. Target and reflecting surface height joint estimation in low-angle radar. *IET Radar Sonar Navig.* **2016**, *10*, 617–623. [\[CrossRef\]](#)
19. Schmidt, R.O. Multiple emitter location and signal parameter estimation. *IEEE Trans. Antennas Propag.* **1986**, *34*, 276–280. [\[CrossRef\]](#)
20. Yin, D.; Zhang, F. Uniform linear array MIMO radar unitary root MUSIC Angle estimation. In Proceedings of the 2020 Chinese Automation Congress (CAC), Shanghai, China, 6–8 November 2020; pp. 578–581. [\[CrossRef\]](#)
21. Roy, R.; Kailath, T. ESPRIT-estimation of signal parameters via rotational invariance techniques. *IEEE Trans. Acoust. Speech Signal Process.* **1989**, *37*, 984–995. [\[CrossRef\]](#)
22. Li, S.; Zhang, Y.; Edwards, R. Two Dimension DOA ESPRIT Algorithm Based on Parallel Coprime Arrays and Complementary Sequence in MIMO Communication System. In Proceedings of the 2019 IEEE International Conference on Signal, Information and Data Processing (ICSIDP), Chongqing, China, 11–13 December 2019; pp. 1–4. [\[CrossRef\]](#)
23. Pillai, S.U.; Kwon, B.H. Forward/backward spatial smoothing techniques for coherent signal identification. *IEEE Trans. Acoust. Speech Signal Process.* **1989**, *37*, 8–15. [\[CrossRef\]](#)
24. Liu, J.; Liu, Z.; Xie, R. Low angle estimation in MIMO radar. *Electron. Lett.* **2010**, *46*, 1565–1566. [\[CrossRef\]](#)
25. Ziskind, I.; Wax, M. Maximum likelihood localization of multiple sources by alternating projection. *IEEE Trans. Acoust. Speech Signal Process.* **1988**, *36*, 1553–1560. [\[CrossRef\]](#)
26. Chen, S.; Zhao, Y.; Hu, Y.; Pang, X. A beamspace maximum likelihood algorithm for target height estimation for a bistatic MIMO radar. *Digit. Signal Process.* **2022**, *122*, 103330. [\[CrossRef\]](#)
27. Lo, T.; Litva, J. Use of a highly deterministic multipath signal model in low-angle tracking. *IEE Proc. F Radar Signal Process.* **1991**, *138*, 163–171. [\[CrossRef\]](#)
28. Bossé, E.; Turner, R.M.; Lecours, M. Tracking swerling fluctuating targets at low altitude over the sea. *IEEE Trans. Aerosp. Electron. Syst.* **1991**, *27*, 806–822. [\[CrossRef\]](#)
29. Zhao, Y.; Pang, X.; Chen, S. A reduced-dimension RML method for transmit beamspace-based MIMO radar. *Digit. Signal Process.* **2021**, *114*, 103072. [\[CrossRef\]](#)
30. Chen, S.; Zhao, Y.; Hu, Y. Beamspace Phase Solving Algorithm for Elevation Angle Estimation. *IEEE Signal Process. Lett.* **2022**, *29*, 742–746. [\[CrossRef\]](#)

31. Anchidin, L.; Mihai, I.V.; Tamas, R.D.; Sharaiha, A. Reflection Coefficient Measurements in the L-Band with Low Directivity Antennas in a Multipath Site. In Proceedings of the 2018 IEEE Conference on Antenna Measurements & Applications (CAMA), Västerås, Sweden, 3–6 September 2018; pp. 1–3. [[CrossRef](#)]
32. Zhang, Y.; Ye, Z.; Liu, C. Estimation of Fading Coefficients in the Presence of Multipath Propagation. *IEEE Trans. Antennas Propag.* **2009**, *57*, 2220–2224. [[CrossRef](#)]
33. Aminu, A.; Secmen, M. Performance evaluation of combined methods for the estimation of fading coefficients of uncorrelated signal sources in multipath propagation. In Proceedings of the 2014 11th International Conference on Electronics, Computer and Computation (ICECCO), Abuja, Nigeria, 29 September–1 October 2014; pp. 1–4. [[CrossRef](#)]
34. Xie, W.; Wen, F.; Liu, J.; Wan, Q. Source Association, DOA, and Fading Coefficients Estimation for Multipath Signals. *IEEE Trans. Signal Process.* **2017**, *65*, 2773–2786. [[CrossRef](#)]
35. Liu, C. Joint fading coefficient and DOA estimation with known waveforms in multipath environment. In Proceedings of the 2011 IEEE CIE International Conference on Radar, Chengdu, China, 24–27 October 2011; pp. 1147–1152. [[CrossRef](#)]
36. Liu, Y.; Liu, H.; Xia, X.G.; Zhang, L.; Jiu, B. Projection Techniques for Altitude Estimation Over Complex Multipath Condition-Based VHF Radar. *IEEE J. Sel. Top. Appl. Earth Obs. Remote Sens.* **2018**, *11*, 2362–2375. [[CrossRef](#)]
37. Song, Y.; Hu, G.; Zheng, G. Height Measurement with Meter Wave MIMO Radar Based on Precise Signal Model under Complex Terrain. *IEEE Access* **2021**, *9*, 49980–49989. [[CrossRef](#)]
38. Liu, Y.; Liu, H.; Jiu, B.; Zhang, L. Altitude Measurement of Low-Angle Target under Complex Terrain Environment for Meter-Wave Radar. In Proceedings of the 2018 IEEE International Conference on Acoustics, Speech and Signal Processing (ICASSP), Calgary, AB, Canada, 15–20 April 2018; pp. 3464–3468. [[CrossRef](#)]
39. Liu, Y.; Jiu, B.; Xia, X.; Liu, H.; Zhang, L. Height Measurement of Low-Angle Target Using MIMO Radar Under Multipath Interference. *IEEE Trans. Aerosp. Electron. Syst.* **2018**, *54*, 808–818. [[CrossRef](#)]
40. Kerr, D.E. *Propagation of Short Radio Waves*, 2nd ed.; Peter Peregrinus Ltd.: London, UK, 1987.
41. Skolnik, I. *Radar Handbook*, 3rd ed.; The McGraw-Hill Companies: New York, NY, USA, 2008.
42. Mahafza, B.R. *Radar Systems Analysis and Design Using Matlab*, 3rd ed.; CRC Press: Boca Raton, FL, USA; London, UK; New York, NY, USA, 2013.
43. Stoica, P.; Nehorai, A. MUSIC, maximum likelihood, and Cramér-Rao bound: Further results and comparisons. In Proceedings of the International Conference on Acoustics, Speech, and Signal Processing, Glasgow, UK, 23–26 May 1989; pp. 2605–2608. [[CrossRef](#)]
44. Boman, K.; Stoica, P. Low Angle Estimation: Models, Methods, and Bounds. *Digit. Signal Process.* **2001**, *11*, 35–79. [[CrossRef](#)]